Available online at www.sciencedirect.com
SCIENCE DIRECT
Journal of Catalysis 229 (2005) 374–388
JOURNAL OF CATALYSIS
www.elsevier.com/locate/jcat

Effect of reductants in N_2O reduction over Fe-MFI catalysts

Takeshi Nobukawa [a], Masanori Yoshida [a], Kazu Okumura [b], Keiichi Tomishige [a,*], Kimio Kunimori [a,*]

[a] *Institute of Materials Science, University of Tsukuba, 1-1-1 Tennodai, Tsukuba, Ibaraki 305-8573, Japan*
[b] *Department of Materials Science, Faculty of Engineering, Tottori University, Koyama-cho Minami, Tottori 680-8552, Japan*

Received 16 September 2004; revised 8 November 2004; accepted 9 November 2004

Available online 23 December 2004

Abstract

We investigated the effect of reductants over ion-exchanged Fe-MFI catalysts (Fe-MFI) based on the catalytic performance in N_2O reduction in the presence and absence of an oxygen atmosphere. In the case of N_2O reduction with hydrocarbons (CH_4, C_2H_6, and C_3H_6) in the presence of excess oxygen, the order of N_2O contribution was as follows: $CH_4 > C_2H_6 > C_3H_6$. This indicates that CH_4 is a more efficient reductant than C_2H_6 and C_3H_6. The TOFs of N_2O decomposition and the N_2O reduction by various reductants (H_2, CO, CH_4) in the absence of oxygen increased with increasing Fe/Al ratio ($Fe/Al \geqslant 0.15$), wheras the TOFs were lower and constant in the range of $Fe/Al \leqslant 0.10$. Temperature-programmed reduction with hydrogen (H_2-TPR) showed that the catalysts with a higher Fe/Al ratio were reduced more easily than those with a lower Fe/Al ratio. Temperature-programmed desorption of O_2 (O_2-TPD) showed that oxygen was desorbed at lower temperatures over the catalysts with a higher Fe/Al ratio. As the result of extended X-ray absorption fine structure (EXAFS) analysis, only mononuclear Fe species were observed over Fe(0.10)-MFI after treatment with N_2O or O_2. On the other hand, binuclear Fe species and mononuclear Fe species were observed over Fe(0.40)-MFI after treatment with N_2O or H_2. More reducible Fe species, which gave lower-temperature O_2 desorption, can be due to Fe binuclear species. Since the N_2O reduction with reductants proceeds via a redox mechanism, the reducible binuclear Fe species can exhibit higher activity. Furthermore, CH_4 can be oxidized by N_2O more easily than can H_2 and CO, although it is generally known that the reactivity of methane is very low.

Keywords: N_2O reduction; Fe-MFI; Fe binuclear; Turnover frequency; Reductant; Wet ion-exchange; EXAFS

1. Introduction

Nitrous oxide (N_2O) has been long considered a relatively harmless gas and has suffered from a lack of interest from environmental scientists and engineers. However, during the last decade there has been a growing concern since N_2O is a harmful gas in our environment, contributing to the greenhouse effect and ozone layer depletion. Therefore, catalytic decomposition of N_2O [1–10] and selective catalytic reduction (SCR) of N_2O with reductants such as hydrocarbons [11–20] and ammonia [21–23] have been proposed as an effective method of N_2O abatement.

Recently, a number of researches have reported that Fe binuclear species are active sites for NO_x SCR and N_2O decomposition on the basis of characterization by means of H_2-TPR, CO-TPR, FTIR, EPR, EXAFS, and Mössbauer spectroscopies [24–32]. Koningsberger et al. [24–26] have reported evidence for a binuclear iron-oxo complex on the basis of EXAFS study of fully exchanged Fe-MFI ($Fe/Al = 1$). They have also proposed the evolution and reactivity of the binuclear iron-oxo species in thermal pretreatment on fully exchanged Fe-MFI prepared by sublimation. Prins et al. [27,28] have reported that the diiron structure resembles the core unit in methane monooxygenase (MMO), in terms of an Fe–Fe distance of approximately 0.3 nm.

* Corresponding authors. Fax: +81-29-855-7440.
E-mail addresses: tomi@tulip.sannet.ne.jp (K. Tomishige), kunimori@ims.tsukuba.ac.jp (K. Kunimori).

0021-9517/$ – see front matter
doi:10.1016/j.jcat.2004.11.009

Joyner and Stockenhuber [33] have shown that the nature of the Fe species in Fe-MFI depends markedly on the ion-exchange method used for the preparation and on the type of pretreatment. On the basis of EXAFS results, these authors reported that in Fe/ZSM-5 zeolites prepared with different ion-exchange methods, Fe was stabilized in different forms, ranging from isolated metal ions to large oxide clusters, and concluded that ion-oxo nanoclusters are most active in the NO_x SCR reaction [33]. On the other hand, mononuclear iron-oxo species, which exist mainly on Fe-MFI with a low exchange level, have been proposed as active species for the reduction of N_2O [13,22]. Delahay et al. [22] have reported that the most active species in the reduction by NH_3 on Fe-BEA in an oxygen-rich atmosphere are in higher proportion at low exchange levels. Furthermore, Segawa et al. [13] have also reported that even low-exchange Fe-ZSM-5 catalysts exhibited high activity when C_3H_6 was used as a reductant.

Recently we reported that the catalytic activity in N_2O reduction with CH_4 on Fe-MFI was dependent on the exchange level of Fe ion [19]. From the results of activity test and catalyst characterization, we have concluded that the active sites are Fe species that are more reducible and give a lower-temperature O_2 desorption peak [19]. From these comparisons, it is expected that the active structure of iron species over zeolites can be influenced by the kinds of reductant. In this study, we investigated the relation between the exchange level of iron and the activity of N_2O reduction with various reductants such as CH_4, C_2H_6, C_3H_6, H_2, and CO. Furthermore, we characterized the structure of Fe species on our Fe-MFI catalysts by means of temperature-programmed desorption of O_2 (O_2-TPD), temperature-programmed reduction with H_2 (H_2-TPR), and extended X-ray absorption fine structure (EXAFS). We discuss the nature of the active sites of N_2O reduction on the basis of the relation between catalyst structure and performance.

2. Experimental

2.1. Catalyst preparation

Fe-MFI catalysts were prepared by an ion-exchange method with an aqueous solution of $FeSO_4 \cdot 7H_2O$ (Wako Pure Chemical Industries Ltd.; 98%) for 20 h at 323 K under a nitrogen atmosphere to avoid the precipitation of $Fe(OH)_3$ [34]. Na-MFI (TOSOH Co.; $SiO_2/Al_2O_3 = 23.8$) was used as the catalyst support. The catalyst was separated from the solution by filtration after an ion exchange procedure. And it was washed thoroughly with distilled water and dried at 383 K overnight, followed by calcination in air at 773 K for 3 h. The loading amount of Fe on MFI was determined by subtraction of the Fe amount in the solution after the separation, analyzed by ICP analysis, from the total amount. The exchange efficiency of $FeSO_4$, the percentage of the iron salt incorporated into the zeolite, was almost 100% in the case of $Fe/Al = 0.05$–0.24. On the other hand, it was almost 80% in the case of $Fe/Al = 0.40$. The catalyst is denoted Fe(X)-MFI, where X stands for the molar ratio of Fe/Al.

Table 1
Reaction conditions in N_2O reduction[a]

Reductant	Gas composition			Catalyst weight (mg)	W/F (g h/mol)
	N_2O (ppm)	Reductant (ppm)	O_2 (%)		
CH_4	950	500	10	50	0.41
C_2H_6	1000	250	10	100	0.41
C_3H_6	1000	250	20	100	0.41
CH_4	950	500	0	50	0.41
H_2	1000	1000	0	100	0.41
CO	1000	1000	0	100	0.41
None	950	0	0	50	0.41

[a] All gases were balanced with He.

2.2. Activity tests

Catalytic reduction of N_2O with various reductants in the presence of excess O_2 or in the absence of O_2 was carried out in a fixed-bed flow reactor. The composition of the reactant gases is listed in Table 1. All of these research-grade gases were purchased from Takachiho Trading Co. Ltd., and they were used without further purification. The catalyst weight was 50 or 100 mg, the total pressure was 0.1 MPa, and W/F (W (g)—catalyst weight, F (mol/h)—total flow rate) was 0.41 g h/mol. The catalysts were pretreated at 773 K with O_2 for 1 h in the reactor. The products were monitored with an on-line TCD gas chromatograph (Shimadzu GC-8A) equipped with a Molecular sieve 5A column for N_2 and O_2 and a Porapak Q column for N_2O; a FID gas chromatograph (Shimadzu GC-14B) equipped with a Gaskuropak 54 column and a methanator for CO, CO_2 and CH_4; and another gas chromatograph equipped with a VZ-10 column for C_2H_6 and C_3H_6. The sampling and analysis of effluent gas was carried out for 1 h at each reaction temperature. The results of the activity tests shown in the figures were obtained under steady-state conditions.

2.3. Catalyst characterization

Temperature-programmed reduction (TPR) with H_2 was performed in a fixed-bed flow reactor. The sample was pretreated in 100% O_2 flow at 773 K for 1 h, and then it was cooled to room temperature and exposed to helium flow to purge the line. The TPR profile of each sample was recorded from room temperature to 973 K under a flow of 5.0% H_2 diluted with Ar. The flow rate of H_2/Ar was 30 ml/min, and the catalyst weight was 50 mg. The heating rate was 10 K/min, and the temperature was maintained kept constant for 10 min after it reached 973 K. The consumption of H_2 was monitored continuously with a TCD gas chromatograph equipped with a Molecular Sieve 5A to remove H_2O from the effluent gas.

Temperature-programmed desorption of O_2 (O_2-TPD) was carried out in a fixed-bed reactor equipped with a quadrupole mass spectrometer (Balzers QMS 200 F). The catalysts (30 mg) were pretreated with O_2 flow (100% O_2, 773 K, 1 h) or N_2O flow (10% N_2O/He, 773 K, 1 h). After the pretreatment, they were cooled to room temperature. Helium gas (flow rate 55 ml/min) was introduced into the reactor, and the sample was heated at a rate of 10 K/min from room temperature to 1273 K. The sample temperature was kept constant for 30 min once it reached 1273 K. Desorbed O_2 in He flow (flow rate, 55 ml/min) was analyzed with a quadrupole mass spectrometer.

2.4. EXAFS measurement and analysis

We prepared the sample for EXAFS measurement by pressing 60 mg of catalyst powder. The thickness of the samples was chosen to be 0.6–0.7 mm (10 mm ϕ) to give an edge jump of 0.2–0.7. The sample was pretreated at 773 K with 11 kPa O_2, H_2, or N_2O for 0.5 h in a closed circulating reactor. After these kinds of pretreatment, we transferred the samples to the measurement cell without exposing the sample disk to air, using a glove box filled with nitrogen.

Fe K-edge XAFS was measured at the BL-12C station of the Photon Factory at the High Energy Accelerator Research Organization in Tsukuba, Japan. The storage ring was operated at 2.5 GeV with a ring current of 300–450 mA. A single Si(111) crystal was used to obtain a monochromatic X-ray beam. The monochromator was detuned to 60% of the maximum intensity to avoid higher harmonics in the X-ray beam. Two ion chambers filled with N_2 and 15% Ar diluted with N_2 were used as detectors of I_0 and I, respectively. EXAFS data were collected in transmission mode at liquid nitrogen temperature. For EXAFS analysis, the oscillation was first extracted from the EXAFS data by a spline smoothing method [35]. The oscillation was normalized by the edge height around 50 eV. The Fourier transformation of the k^3-weighted EXAFS oscillation from k space to r space was performed over the range 23–120 nm^{-1} to obtain a radial distribution function. The inversely Fourier filtered data were analyzed by a common curve-fitting method [36,37]. For the curve-fitting analysis, the empirical phase shift and amplitude functions for Fe–O were extracted from the data for ferric acetylacetonate. The phase shift and backscattering amplitude of Fe–Si and Fe–Fe bonds were calculated with the software FEFF8.2 [38]. The program ATOMS [39] was used to calculate coordination numbers and interatomic distances from reported XRD data for reference compounds. The theoretical Fe–Fe reference was calibrated against EXAFS data obtained from Fe_2O_3 (hematite) at liq-

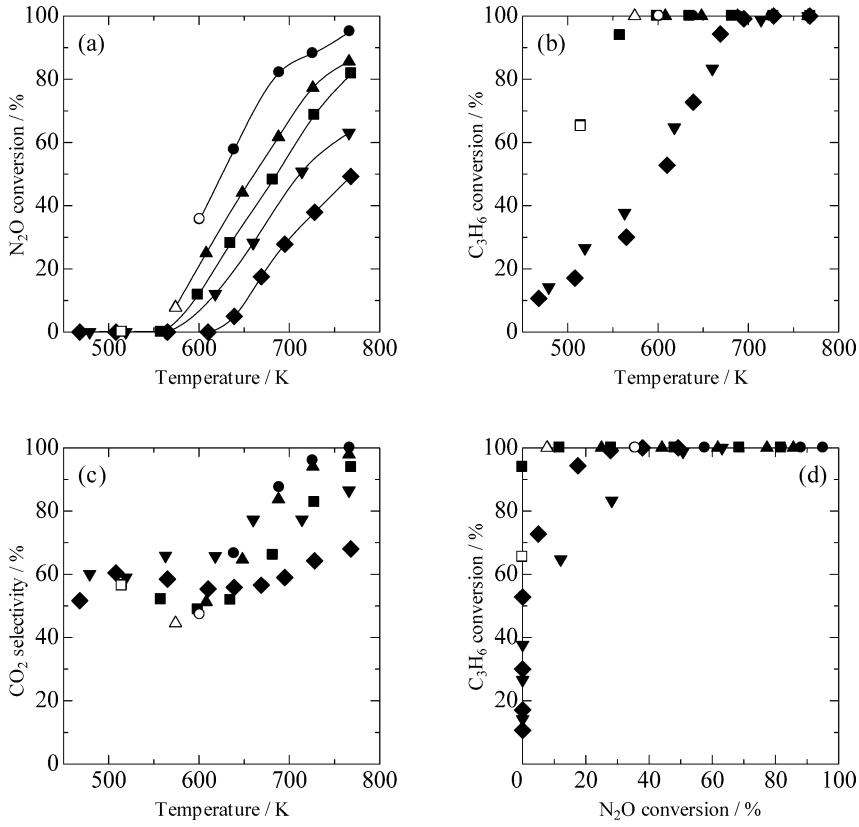

Fig. 1. Reaction temperature dependence of catalyst performance of Fe-MFI catalyst in N_2O reduction with C_3H_6 under excess O_2 atmosphere: (a) N_2O conversion, (b) C_3H_6 conversion, (c) CO_2 selectivity ($CO_2/(CO + CO_2)$), and (d) C_3H_6 conversion as function of N_2O conversion. ●: Fe(0.40)-MFI, ▲: Fe(0.24)-MFI, ■: Fe(0.15)-MFI, ▼: Fe(0.10)-MFI, and ◆: Fe(0.05)-MFI. Gas composition: 1000 ppm N_2O, 250 ppm C_3H_6, 20% O_2 (He balance). Open marks represent the data at which carbon deposition was observed.

uid nitrogen temperature, by fitting in *R* space. EXAFS data were analyzed with the REX2000 program (Rigaku Co.; Version 2.3.3).

3. Results and discussion

3.1. N_2O reduction with hydrocarbons over Fe-MFI under an excess oxygen atmosphere

Fig. 1 shows the temperature dependence of the catalyst performance of Fe-MFI in N_2O reduction with C_3H_6 under an excess oxygen atmosphere. In this experiment, the activity test was carried out from high temperature (773 K) to low temperature (at most 473 K) to avoid the influence of carbon deposition, which was observed at lower temperature (open symbols in Fig. 1a). In this temperature region, the color of the catalyst became black during the reaction, and a disagreement in the carbon mass balance was observed. The introduced carbon amount did not agree with the carbon amount in the effluent gas at the lower temperature described by open marks. This behavior due to carbon deposition was reported previously [40]. In addition, we confirmed the carbon deposition on the catalyst after reaction by thermogravimetry analysis (TGA). In TGA, the weight loss due to coke combustion was observed during heating under an air atmosphere. On the other hand, for the data indicated by closed symbols in Fig. 1, the mass balance was good. N_2O conversion increased with the loading amount of Fe. According to Fig. 1b, C_3H_6 conversion increased with reaction temperature over Fe-MFI with low loading of Fe (Fe/Al = 0.05 and 0.10). In contrast, C_3H_6 conversion reached almost 100% in a rather low temperature range over Fe-MFI (Fe/Al = 0.15 and 0.24). CO_2 and CO were observed as the carbon-containing products, and CO_2 selectivity is represented in Fig. 1c. Fig. 1d shows the relation between N_2O conversion and C_3H_6 conversion. It is clearly shown that C_3H_6 conversion reached 100%, even for a low level of N_2O conversion. Furthermore, C_3H_6 conversion was observed even when N_2O conversion was zero, which means that C_3H_6 reacted with oxygen, not with N_2O.

Fig. 2 shows the temperature dependence of the catalyst performance of Fe-MFI in N_2O reduction with C_2H_6 under an excess oxygen atmosphere. N_2O and C_2H_6 conversions increased with reaction temperature and the loading amount of Fe (Figs. 2a and 2b). In the relation between N_2O and the reductant conversion, the behavior in N_2O reduction with C_2H_6 was much different from that in N_2O reduction with C_3H_6. As shown in Fig. 2d, C_2H_6 conversion increases proportionally with N_2O conversion in a N_2O conversion range of 0–50%. This means that C_2H_6 conversion is almost zero

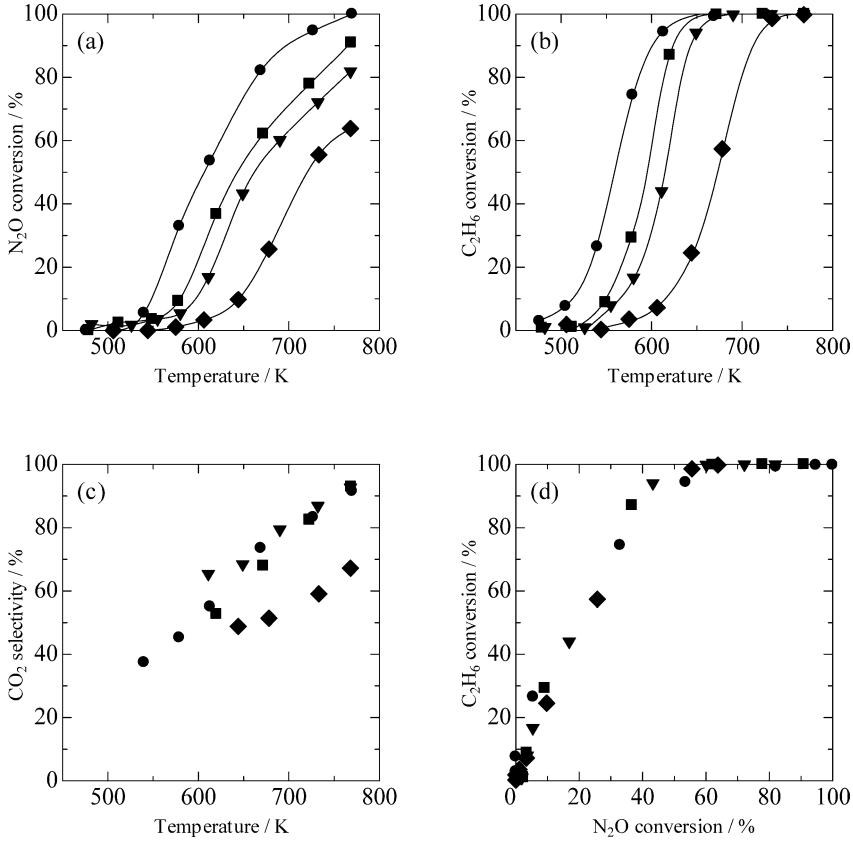

Fig. 2. Reaction temperature dependence of catalyst performance of Fe-MFI catalyst in N_2O reduction with C_2H_6 under excess O_2 atmosphere: (a) N_2O conversion, (b) C_2H_6 conversion, (c) CO_2 selectivity ($CO_2/(CO + CO_2)$), and (d) C_2H_6 conversion as function of N_2O conversion. ●: Fe(0.40)-MFI, ■: Fe(0.15)-MFI, ▼: Fe(0.10)-MFI, and ◆: Fe(0.05)-MFI. Gas composition: 1000 ppm N_2O, 250 ppm C_2H_6, 10% O_2 (He balance).

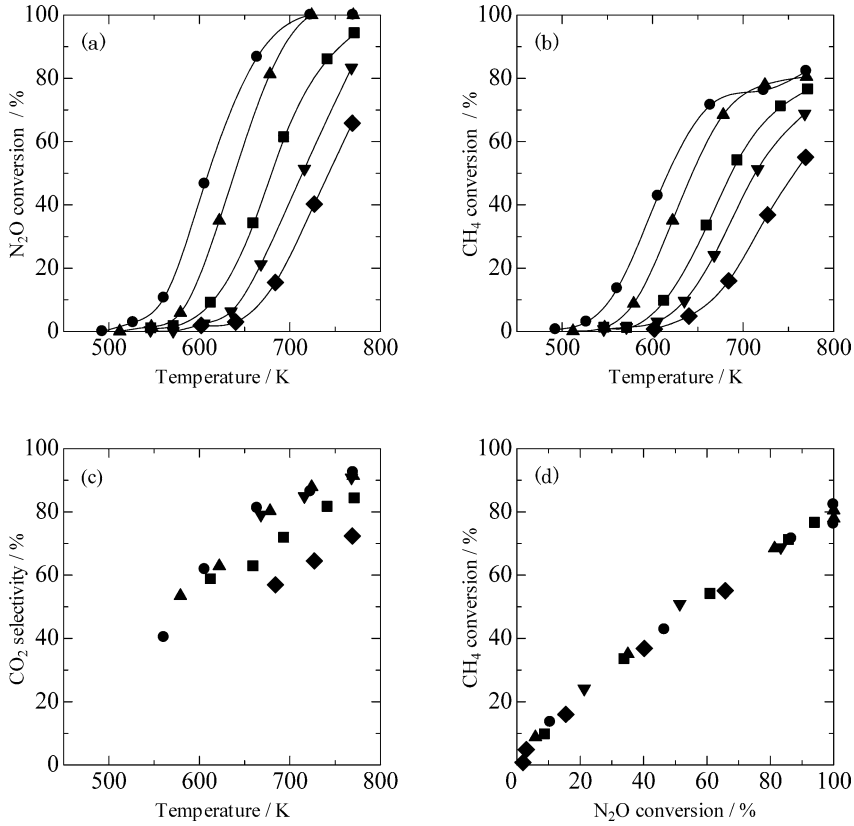

Fig. 3. Reaction temperature dependence of catalyst performance of Fe-MFI catalyst in N_2O reduction with CH_4 under excess O_2 atmosphere: (a) N_2O conversion, (b) CH_4 conversion, (c) CO_2 selectivity ($CO_2/(CO+CO_2)$), and (d) CH_4 conversion as function of N_2O conversion. ●: Fe(0.40)-MFI, ▲: Fe(0.24)-MFI, ■: Fe(0.15)-MFI, ▼: Fe(0.10)-MFI, and ◆: Fe(0.05)-MFI. Gas composition: 950 ppm N_2O, 500 ppm CH_4, 10% O_2 (He balance).

when N_2O conversion is zero. This suggests that N_2O is necessary for the activation of C_2H_6. Similar behavior was also observed on the Fe-BEA catalyst in our previous study [17]. In addition, the carbon amount in the effluent gas was balanced with that introduced in the case of C_2H_6 in all temperature ranges, unlike the case of C_3H_6.

Fig. 3 shows the temperature dependence of catalyst performance in N_2O reduction with CH_4 under an excess oxygen atmosphere. Conversions of N_2O and CH_4 increased with Fe amount (Figs. 3a and 3b). It is known that CH_4 is less reactive than C_2H_6 and C_3H_6. However, N_2O reduction with CH_4 started at almost the same temperature as that with C_2H_6 and C_3H_6. For example, the reduction of N_2O started at almost the same temperature (about 523 K) over Fe(0.40)-MFI in the case of CH_4 and C_2H_6. It is characteristic that N_2O conversion in Fig. 3a reached 100% at about 700 K over Fe(0.40)-MFI in the case of N_2O reduction with CH_4. In contrast, in the case of N_2O reduction with C_2H_6 and C_3H_6, N_2O conversion did not reach about 100% below ca. 760 K (Figs. 1a and 2a). In addition, it should be pointed out that there was a plateau in CH_4 conversion at which N_2O conversion reached 100% (Fig. 3b), especially over Fe-MFI ($Fe/Al = 0.40$). This indicates that CH_4 cannot react directly with O_2, even at 700 K. These results indicate that CH_4 is the most efficient reductant for the SCR of N_2O. Since the feeding ratio of hydrocarbons to N_2O is higher than the stoichiometry of N_2O reduction with hydrocarbons, as listed in Table 1, N_2O conversion can reach 100% before the conversion of hydrocarbons when the reaction proceeds stoichiometrically. However, this is not the case when hydrocarbons react with oxygen, and this tendency is related to the reactivity between hydrocarbons and oxygen. Therefore, for evaluation of the contribution of N_2O in a total oxidizing agent, the results are shown in Fig. 4. In the case of N_2O reduction with CH_4, the contribution of N_2O can be calculated by (consumed N_2O)/($4CO_2 + 3CO$) on the basis of these equations:

$$CH_4 + 4[O] \rightarrow CO_2 + 2H_2O,$$
$$CH_4 + 3[O] \rightarrow CO + 2H_2O,$$

[O]: oxygen atom originating from N_2O and O_2.

The details of C_2H_6 and C_3H_6 are referred to in the caption of Fig. 4. On both Fe-MFI catalysts, the N_2O contribution to the $N_2O/CH_4/O_2$ system is higher than that in the case of the $N_2O/C_2H_6/O_2$ and $N_2O/C_3H_6/O_2$ systems. This indicates that CH_4 reacted with N_2O more efficiently than did C_2H_6 and C_3H_6. In other words, a higher concentration of reductants must be supplied for higher N_2O conversion and removal in the case of C_2H_6 and C_3H_6 compared with CH_4. From these viewpoints, CH_4 is a more suitable reductant when N_2O is removed from containing air. In terms of the practical aspect, the suitability of hydrocarbons as a N_2O

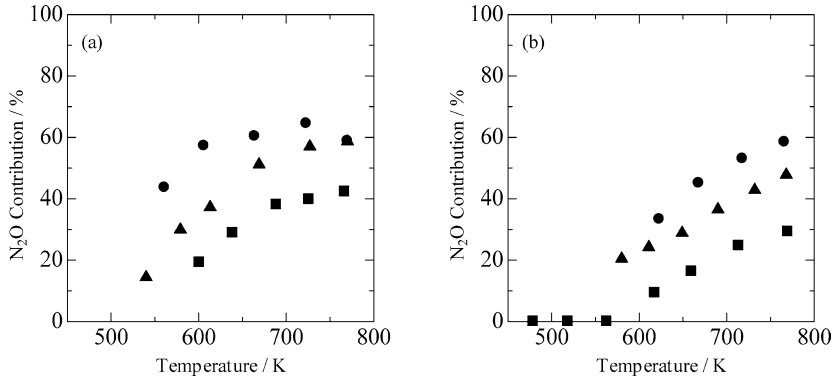

Fig. 4. N_2O contribution in total oxidizing agents during N_2O reduction with various hydrocarbons under excess oxygen atmosphere: (a) Fe(0.40)-MFI and (b) Fe(0.10)-MFI. ●: CH_4, ▲: C_2H_6, and ■: C_3H_6. The reaction of CO and CO_2 formation is assumed below, $C_mH_n + (m + n/2)[O] \rightarrow mCO + (n/2)H_2O$, $C_mH_n + (2m + n/2)[O] \rightarrow mCO_2 + (n/2)H_2O$. On the basis of the assumptions, N_2O contribution is calculated as follows. N_2O contribution = (consumed N_2O)/$((1 + n/2m)CO + (2 + n/2m)CO_2)$.

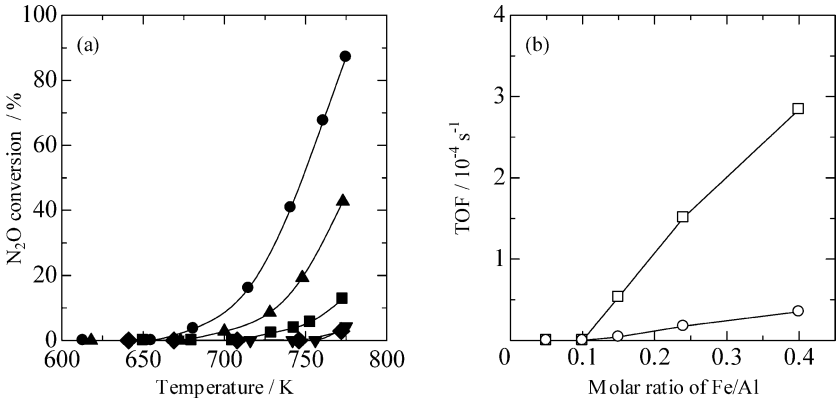

Fig. 5. Reaction temperature dependence of catalyst performance of Fe-MFI catalyst in N_2O decomposition in the absence of O_2: (a) N_2O conversion; ●: Fe(0.40)-MFI, ▲: Fe(0.24)-MFI, ■: Fe(0.15)-MFI, ▼: Fe(0.10)-MFI, and ◆: Fe(0.05)-MFI. (b) TOF as a function of molar ratio of Fe/Al; ○: 673 K, □: 723 K. Gas composition: 950 ppm N_2O (He balance).

reductant can be estimated as follows: $CH_4 > C_2H_6 > C_3H_6$ on the basis of the order of N_2O contribution. In addition, N_2O conversion was almost proportional to CH_4 conversion, as shown in Fig. 3d, and the line goes through the origin. This also suggests that N_2O is necessary for the activation of CH_4. On the other hand, C_3H_6 can be activated without N_2O on the basis of the result in Fig. 1d. In the three reactions, Fe-MFI with higher Fe loading exhibited higher activity. The relation between the activity and Fe loading is discussed in detail in the next section. From these results, we can conclude that CH_4 is superior to C_2H_6 and C_3H_6 in N_2O reduction with hydrocarbons under an excess oxygen atmosphere.

3.2. Reaction of N_2O with various reductants over Fe-MFI catalysts

In the previous section we described the activity test, carried out in the presence of an excess oxygen atmosphere. We did this because N_2O should be removed from the gas containing air in the practical process. In contrast, in this section we describe the activity test as it is carried out in the absence of oxygen. We do this because it is possible to exclude the reaction of the reductant with oxygen in order to investigate the effect of a reductant in N_2O reduction. Reaction temperature dependence in N_2O decomposition over Fe-MFI catalysts is shown in Fig. 5. These results are also based on the activity under steady-state conditions. Therefore, the product N_2/O_2 ratio was 2:1, which means that the reaction proceeded stoichiometrically. N_2O conversion was dependent on Fe loading. Furthermore, the starting temperature was also influenced by Fe loading. This behavior can be related to the O_2 desorption temperature in O_2-TPD profiles. The starting temperature of oxygen desorption in O_2-TPD profiles became lower over Fe-MFI with higher Fe loading. As shown in Fig. 6, the starting temperature of O_2 desorption can be estimated to be 670 K and 790 K over Fe(0.40)-MFI and Fe(0.10)-MFI, respectively. The temperature at which N_2O decomposition starts to proceed corresponds well with the temperatures in O_2-TPD of N_2O-treated catalysts. This suggests that the rate-limiting step of N_2O decomposition is oxygen desorption from the catalyst surface. This is also supported by previous reports [10,41,42]. Fig. 5b shows turnover frequency (TOF) of N_2O decomposition as a function of the molar ratio of Fe/Al in Fe-MFI. It is found that

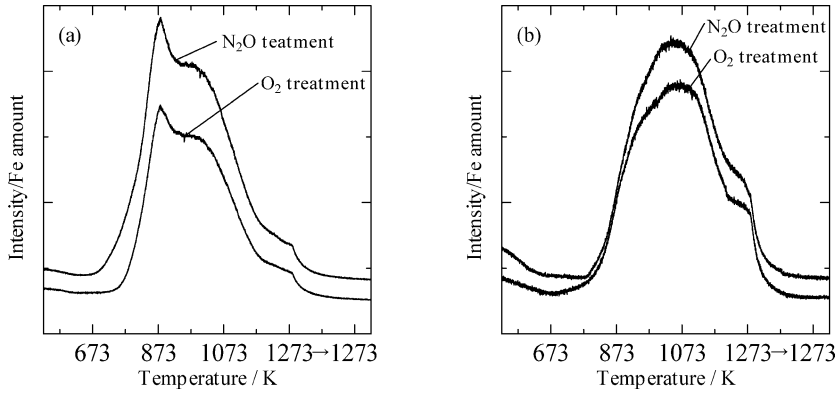

Fig. 6. Temperature-programmed desorption of oxygen after O_2 and N_2O treatments normalized by Fe loading amount: (a) Fe(0.40)-MFI and (b) Fe(0.10)-MFI. Reaction temperature: from room temperature to 1273 K, 10 K/min, 30 min hold. Gas composition: He, 55 ml/min. Catalyst weight: 30 mg. Pretreatment: 100% O_2 flow, 773 K, 1 h, or 10% N_2O/He flow, 773 K, 1 h.

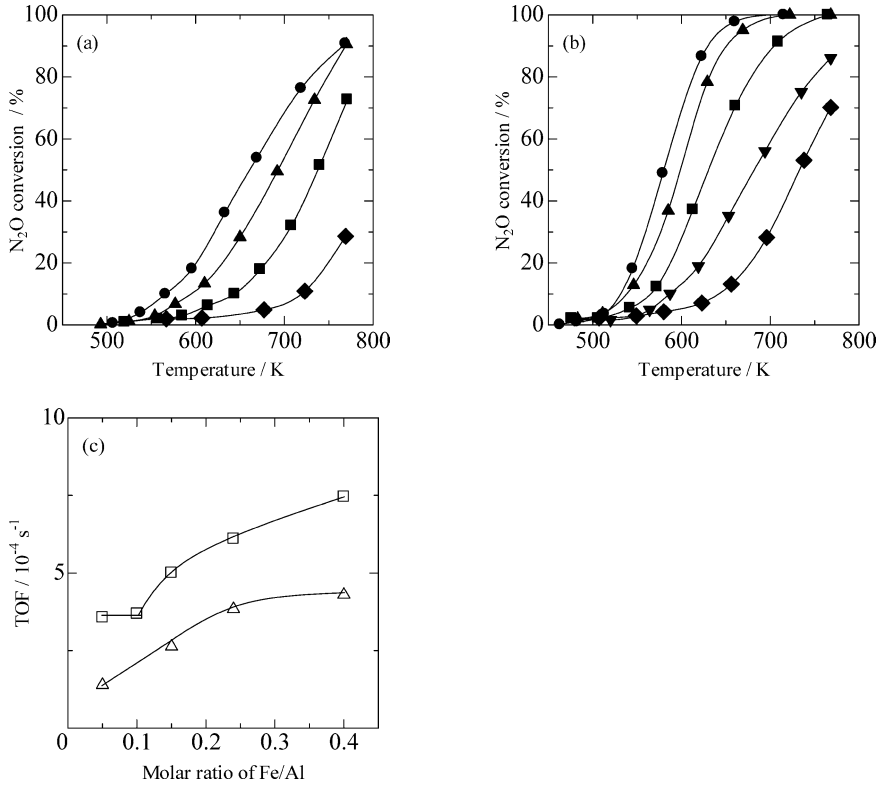

Fig. 7. Reaction temperature dependence of N_2O conversion of Fe-MFI catalyst in N_2O reduction with H_2 and CO in the absence of O_2: (a) H_2, (b) CO, and (c) TOF as a function of molar ratio of Fe/Al calculated at 573 K (□: CO) and 623 K (△: H_2). ●: Fe(0.40)-MFI, ▲: Fe(0.24)-MFI, ■: Fe(0.15)-MFI, ▼: Fe(0.10)-MFI, and ◆: Fe(0.05)-MFI. Gas composition: (a) 1000 ppm N_2O, 1000 ppm H_2 (He balance), and (b) 1000 ppm N_2O, 1000 ppm CO (He balance).

the TOF of N_2O decomposition at 673 K was almost zero in the range of Fe/Al $\leqslant$ 0.10; however, the TOF drastically increased with Fe loading (Fe/Al $>$ 0.10). The profile of O_2-TPD over Fe(0.10)-MFI gave only one peak. In contrast, another sharp peak at a lower desorption temperature ($\sim$ 873 K) appeared over Fe(0.40)-MFI (Fig. 6a). This kind of Fe species can contribute to the high catalytic activity over Fe(0.40)-MFI. The behavior of TOF can be explained by the Fe species that gave the lower-temperature peak. As shown in Fig. 6a, the amount of O_2 desorption after N_2O treatment was larger than that after O_2 treatment, the origin of which has been discussed extensively in our previous report [19].

Fig. 7(a) shows the temperature dependence of N_2O conversion in N_2O reduction with H_2. N_2O conversion in the $N_2O + H_2$ reaction was much higher than that in N_2O decomposition. Catalytic activity and the temperature at which the $N_2O + H_2$ reaction started was also dependent on the loading amount of Fe. Fig. 8 shows the profiles of temperature-programmed reduction (TPR) of Fe-MFI after O_2 treatment. Fe-MFI (Fe/Al = 0.05 and 0.1) started

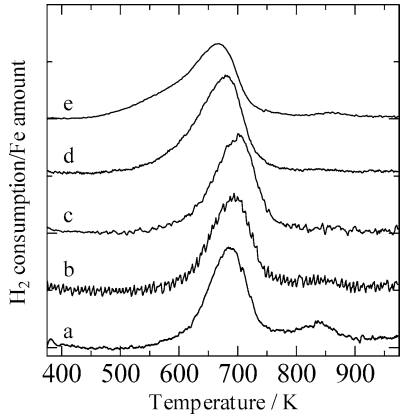

Fig. 8. Temperature-programmed reduction in hydrogen over Fe-MFI catalysts normalized by Fe loading amount: (a) Fe(0.05)-MFI, (b) Fe (0.10)-MFI, (c) Fe(0.15)-MFI, (d) Fe(0.24)-MFI, and (e) Fe(0.40)-MFI. Reaction temperature: from room temperature to 973 K, 10 K/min. Gas composition: 5.0% H_2/Ar, 30 ml/min. Catalyst weight: 50 mg. Pretreatment: 100% O_2 flow, 773 K, 1 h.

to be reduced in H_2 at about 600 K. In contrast, Fe-MFI (Fe/Al = 0.15–0.40) started to be reduced at a lower temperature than Fe-MFI (Fe/Al = 0.05 and 0.10). For example, the reduction started at 450 K on Fe(0.40)-MFI. This suggests that Fe-MFI catalysts with higher Fe loading contain more reducible Fe species. The tendency in H_2-TPR is similar to that in $N_2O + H_2$. Although the difference in starting temperatures between H_2-TPR and the $N_2O + H_2$ reaction was clearly observed, it is thought to be explained by the pressure difference. Fig. 7b shows the result of N_2O reduction with CO. Although N_2O conversion in the $N_2O + CO$ reaction was higher than that of $N_2O + H_2$ reduction, the tendency of the $N_2O + CO$ reaction was similar to that of the $N_2O + H_2$ reaction. The relations between the TOF value and the Fe/Al ratio are shown Fig. 7(c). The TOFs of $N_2O + H_2$ and the $N_2O + CO$ reaction increased with increasing Fe/Al, which can be interpreted on the basis of TPR profiles. More reducible Fe species can work as the active site at lower reaction temperatures. The amount of more reducible Fe species increased with increasing Fe loading, and this can explain the relations between the TOFs and Fe/Al.

Fig. 9 shows the temperature dependence in N_2O reduction with CH_4 in the absence of oxygen. The carbon amount in the effluent was balanced with that introduced in this reaction. This means that the results correspond to the steady-state activity and coke was not deposited. Although the details are not shown here, a large amount of coke was deposited in the $N_2O + C_2H_6$ and $N_2O + C_3H_6$ reactions in the absence of excess oxygen. From this viewpoint, the data in the case of C_2H_6 and C_3H_6 were not available under this type of conditions. CH_4 conversion had a plateau

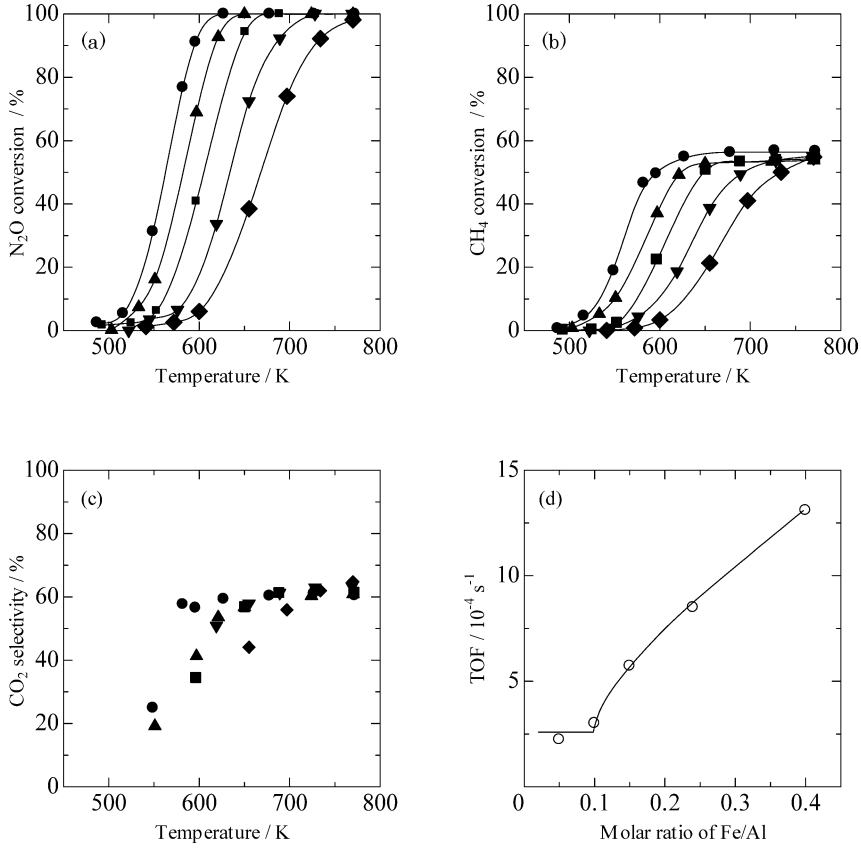

Fig. 9. Reaction temperature dependence of catalyst performance of Fe-MFI catalyst in N_2O reduction with CH_4 in the absence of O_2: (a) N_2O conversion, (b) CH_4 conversion, (c) CO_2 selectivity, (d) TOF calculated at 573 K. ●: Fe(0.40)-MFI, ▲: Fe(0.24)-MFI, ■: Fe(0.15)-MFI, ▼: Fe(0.10)-MFI, and ◆: Fe(0.05)-MFI. Gas composition: 950 ppm N_2O, 500 ppm CH_4 (He balance).

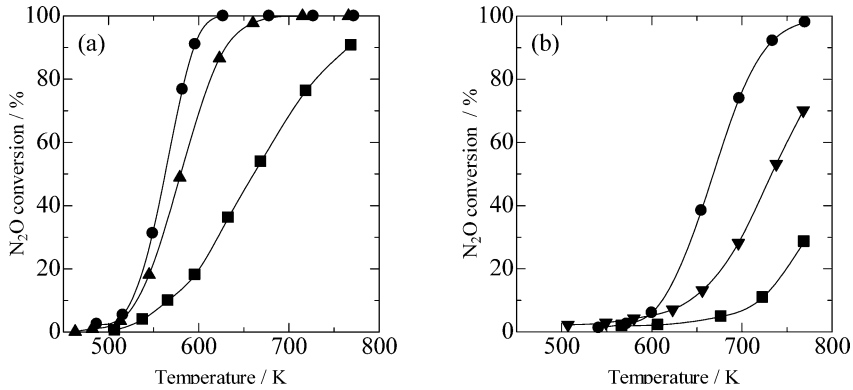

Fig. 10. Comparison of N_2O conversion in N_2O reduction with various reductants in the absence of O_2 over Fe-MFI catalysts: (a) Fe(0.40)-MFI and (b) Fe(0.05)-MFI. ●: CH_4, ▲: CO, ■: H_2. Reaction conditions were shown in the figure caption in Figs. 7 and 9.

since N_2O conversion reached almost 100%. These profiles are also observed in N_2O reduction with CH_4 in the presence of excess oxygen. The temperature at which the $N_2O + CH_4$ reaction started was also dependent on Fe loading, and the tendency is also observed in the $N_2O + H_2$ and $N_2O + CO$ reactions. Fig. 9d shows the relation between the TOF of the $N_2O + CH_4$ reaction and Fe/Al. The TOF value jumped at Fe/Al = 0.15 and increased with increasing Fe/Al. This TOF behavior is similar to that in the $N_2O + H_2$ and $N_2O + CO$ reactions. It is suggested that more reducible Fe species can also contribute to the enhancement of TOF in the case of the $N_2O + CH_4$ reaction.

Fig. 10 shows the comparison of N_2O conversion in various reactions over Fe(0.40)-MFI and Fe(0.05)-MFI. The order of N_2O conversion over Fe(0.40)-MFI and Fe(0.05)-MFI was $CH_4 > CO > H_2$ in all temperature ranges. It should be noted that the $N_2O + CH_4$ reaction gave the highest N_2O conversion over all of the catalysts and in all temperature ranges. Considering that the reactivity of methane is generally much lower than those of H_2 and CO, it is very interesting that methane has a higher reactivity than H_2 and CO for N_2O reduction. According to the results of TOF in various reactions, the structure of the active sites is almost the same on Fe-MFI (Fe/Al = 0.05 and 0.10) catalysts, and other active sites appear on Fe-MFI (Fe/Al = 0.15–0.40), which are more reducible iron species.

3.3. Fe K-edge EXAFS analysis after different treatment

We carried out a structural analysis of the Fe(0.10)-MFI and Fe(0.40)-MFI catalysts with some treatments on the basis of the results from O_2-TPD by means of EXAFS. Figs. 11a and 11b show the Fe *K*-edge EXAFS oscillations for Fe(0.10)-MFI measured after treatment with O_2 or N_2O. It seems that the oscillation on Fe(0.10)-MFI treated with O_2 is similar to that with N_2O. As shown in Fig. 6b, only one O_2 desorption peak was observed on Fe(0.10)-MFI, and the desorption profile of the sample after O_2 treatment was almost the same as that after N_2O treatment. This means that the additional oxygen deposition by N_2O treatment did not occur on Fe(0.10)-MFI. This can explain the similarity of the spectra. The Fourier transforms (FTs) of k^3-weighted EXAFS oscillations for Fe(0.10)-MFI are shown in Fig. 11c, and their fitting results are shown in Figs. 11d and 11e. The details of the curve-fitting parameters are listed in Table 2. Two major peaks were observed in the regions of 0.1–0.2 nm and 0.2–0.3 nm in FT spectra. One peak with a shorter bond length of 0.1–0.2 nm can be assigned to the Fe–O bond, which has already been reported in EXAFS studies [25,27,43]. And the other peak, with a longer bond length of 0.2–0.3 nm, can be assigned to the Fe–Si bond, as shown later. In the O_2-TPD profile of Fe(0.10)-MFI, the amount of O_2 desorption from O_2- and N_2O-treated samples is estimated to be $O_2/Fe = 0.16$ and 0.17, respectively. These values are less than $O_2/Fe = 0.25$, which is based on the equation

$$4Fe^{3+} + 2O^{2-} \rightarrow 4Fe^{2+} + O_2.$$

This suggests that a part of Fe can produce oxygen desorption, and the other cannot. Therefore, it is expected that there are two kinds of Fe–O bond on the basis of the amount of O_2 desorption. This suggestion led us to use two kinds of Fe–O bond in the curve-fitting analysis (Table 2).

The Fe–O bond, with a shorter distance of 0.187 nm, can be ascribed to O atoms of the OH species coordinated with Fe ion species. In previous reports, Koningsberger et al. [25,26] assigned an Fe–O distance of 0.188 nm to a terminal OH group and an Fe–O distance of 0.193 nm to the bridging Fe–O–Fe oxygen atom. The Fe–O bond, with a longer distance of 0.204 nm, is ascribed to O atoms in the zeolite lattice, by which the Fe atoms are stabilized to the zeolite lattice as Fe–O–Si and Fe–O–Al, and it is expected that the oxygen species are difficult to desorb. This is supported by previous reports [25,28].

From the fitting results of EXAFS data, we could fit our spectra with the Fe–Si shell. Joyner et al. [33] have reported that the distance of the Fe–Si shell is about 0.32 nm, which is almost the same as our result. On the other hand, Choi et al. [43] reported EXAFS analysis of Fe-ZSM-5 prepared by solid ion exchange, and they assigned the peak between 0.25 and 0.30 nm to the Fe–Al bond. Generally speaking, it is difficult to distinguish between Al and Si as a backscattering atom because the difference in atomic number is very

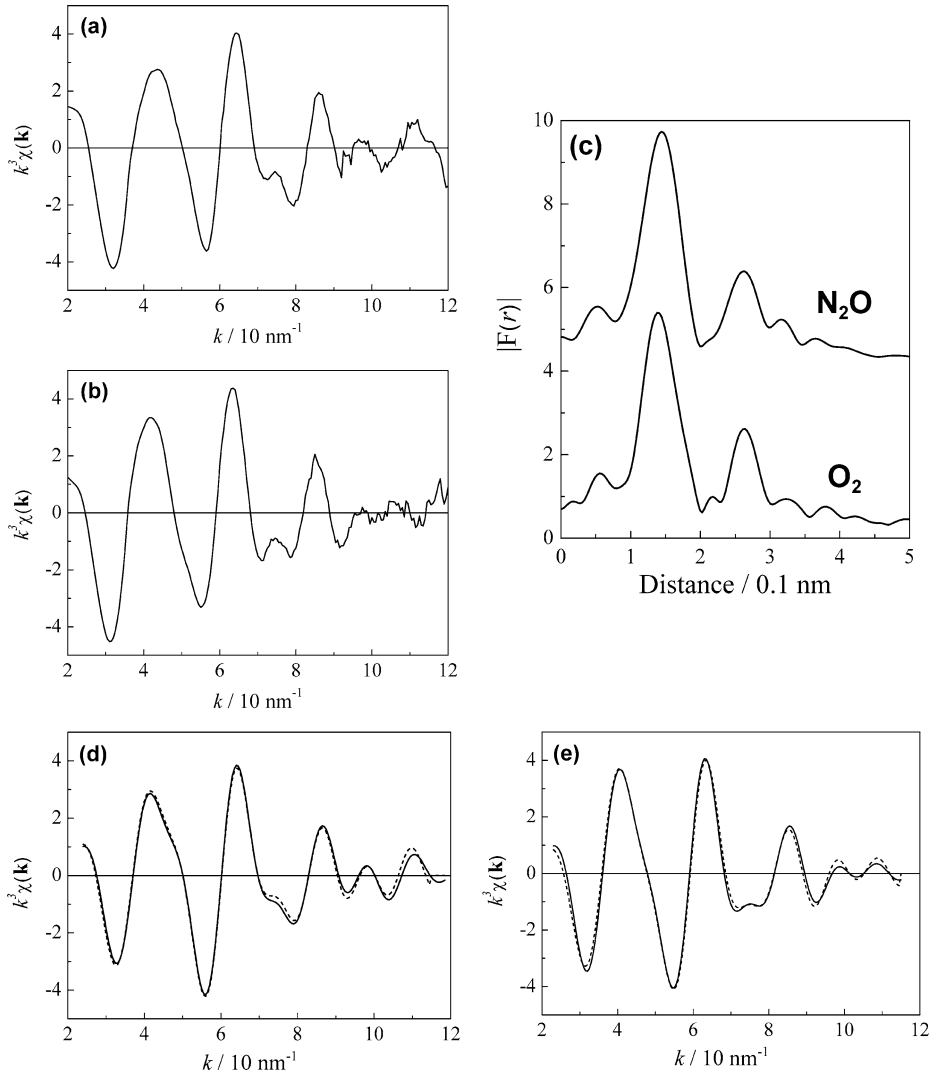

Fig. 11. (a, b): k^3-weighted Fe K-edge EXAFS for Fe(0.10)-MFI catalyst after treatment with (a) O_2 or (b) N_2O. (c): Fourier transform of k^3-weighted Fe K-edge EXAFS for Fe(0.10)-MFI catalyst after treatment with O_2 (Fourier transform range: 25–115 nm^{-1}) or N_2O (Fourier transform range: 23–115 nm^{-1}). (d, e): Fourier filtered EXAFS data (solid line) and calculated data (dotted line) of Fe(0.10)-MFI after treatment with (d) O_2 or (e) N_2O. Fitting results are listed in Table 2.

Table 2
Fe K-edge EXAFS fitting results for Fe(0.10)-MFI catalyst pretreated under different conditions

Shells	CN[a]	R[b] ($\times 10^{-1}$ nm)	σ[c] ($\times 10^{-1}$ nm)	ΔE_0[d] (eV)	R_f[e] (%)
Fitting results of Fe(0.10)-MFI after O_2 treatment[f]					
Fe–O_1	1.7 ± 0.1	1.87 ± 0.01	0.041 ± 0.012	-0.1 ± 0.8	0.69
Fe–O_2	1.7 ± 0.1	2.04 ± 0.01	0.045 ± 0.015	3.8 ± 0.9	
Fe–Si	1.9 ± 0.2	3.17 ± 0.01	0.058 ± 0.018	-5.6 ± 1.0	
Fitting results of Fe(0.10)-MFI after N_2O treatment[g]					
Fe–O_1	1.6 ± 0.1	1.88 ± 0.01	0.064 ± 0.011	-5.8 ± 1.0	1.09
Fe–O_2	2.0 ± 0.1	2.04 ± 0.01	0.070 ± 0.011	3.1 ± 0.9	
Fe–Si	1.9 ± 0.2	3.19 ± 0.01	0.066 ± 0.018	-4.7 ± 1.1	

[a] Coordination number.
[b] Distance.
[c] Debye–Waller factor.
[d] Difference in the origin of photoelectron energy between the reference and the sample.
[e] Residual factor.
[f] Fourier filtering range: 0.083–0.304 nm.
[g] Fourier filtering range: 0.077–0.304 nm.

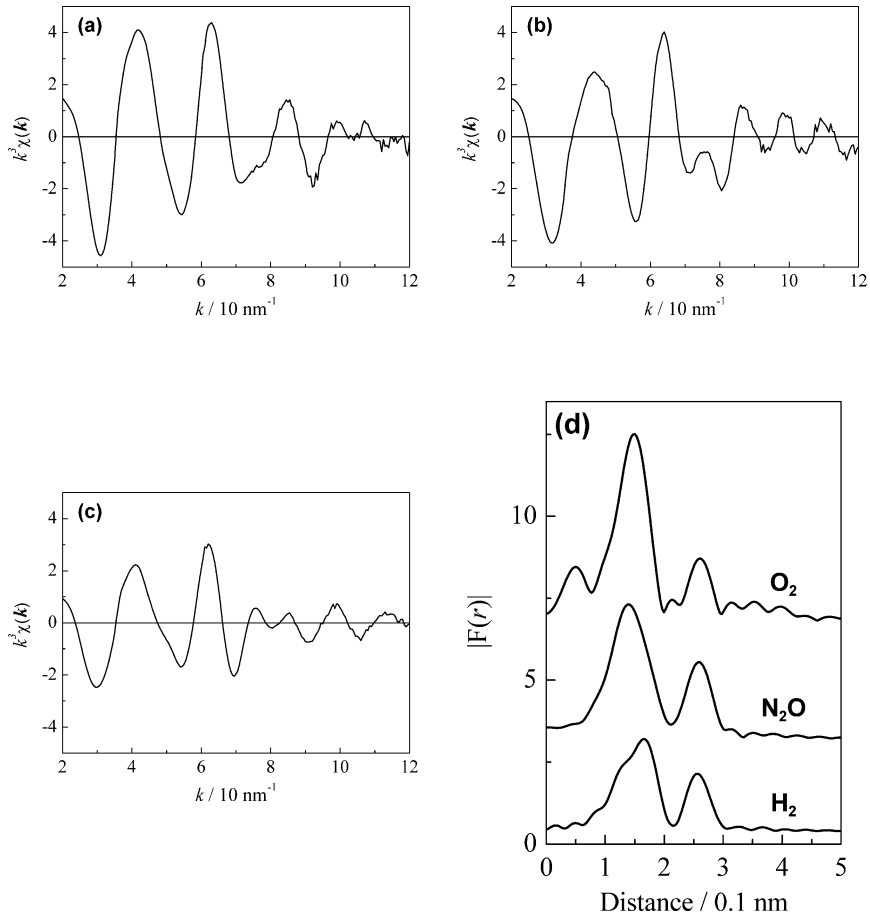

Fig. 12. k^3-weighted Fe K-edge EXAFS for Fe(0.40)-MFI catalyst after treatments with (a) O_2, (b) N_2O, and (c) H_2. (d) Fourier transform of k^3-weighted Fe K-edge EXAFS for Fe(0.40)-MFI catalyst after treatments with O_2, N_2O, and H_2. Fourier transform range: 24–115 nm^{-1}.

small. However, this tendency can be explained by the local structure of Fe on MFI. It has been proposed that an Fe ion over the acid site is neighboring one Al and two or more Si atoms through the lattice oxygen atoms. This suggests that the Si atoms make a greater contribution than the Al atom. The possibility of an Fe–Fe bond over Fe(0.10)-MFI cannot be accepted, because this catalyst contains Fe ions almost exclusively, with lower reducibility from H_2-TPR and O_2-TPD results (Figs. 6b and 8). In addition, the Fe loading of the Fe(0.10)-MFI catalyst is low, and because the catalyst was prepared by severely controlled wet ion exchange, it is expected that the Fe species over the Fe(0.10)-MFI catalyst can be isolated. In fact, it is difficult to fit the FT peak with one wave of Fe–Fe. From these comparisons, for the Fe(0.10)-MFI after O_2 treatment, three-shell fitting (Fe–O_1, Fe–O_2, Fe–Si) gave the appropriate result. The comparison of the results for the O_2 and N_2O treatments shows that the coordination number and the distance were almost the same values. This also shows that N_2O treatment did not lead to a structural change in the Fe species.

Figs. 12a–12c show EXAFS oscillations for Fe(0.40)-MFI after the treatments with O_2, N_2O, and H_2. It is found that the oscillation of Fe(0.40)-MFI after N_2O treatment is different from that after O_2 treatment, especially in the higher k region. In addition, it was also found that the oscillations of Fe(0.40)-MFI are similar to that of Fe(0.10)-MFI in the case of O_2 treatment. The FT spectra of k^3-weighted EXAFS oscillations for Fe(0.40)-MFI with different treatments are shown in Fig. 12d. Their fitting results are shown in Figs. 13a–13c and listed in Table 3. Regarding Fe(0.40)-MFI after O_2 treatment, the curve fitting was carried out on the basis of the results of Fe(0.10)-MFI because of the similarities in EXAFS oscillations. Curve-fitting results for these two samples were also similar. In addition, a different point is the length of the short Fe–O_1 bond. It seems that the length of the Fe–O_1 bond in Fe(0.40)-MFI is a little longer than that in Fe(0.10)-MFI. Koningsberger et al. [26] have reported that the Fe–O distance of Fe–O–Fe bridged oxygen (0.193 nm) is longer than that of terminal OH species (0.188 nm). In our case, although the difference in the bond distance is not so large, we think that the contribution of the bridged oxygen species can be added to the bond of Fe–O_1 on Fe(0.40)-MFI. This interpretation can be supported by the O_2-TPD profiles (Fig. 6). In the case of Fe(0.40)-MFI after O_2 treatment, a desorption peak was observed at lower temperatures, and this was not observed over Fe(0.10)-MFI. This indicates that Fe(0.40)-MFI has oxygen species different from that of Fe(0.10)-MFI, which can be desorbed

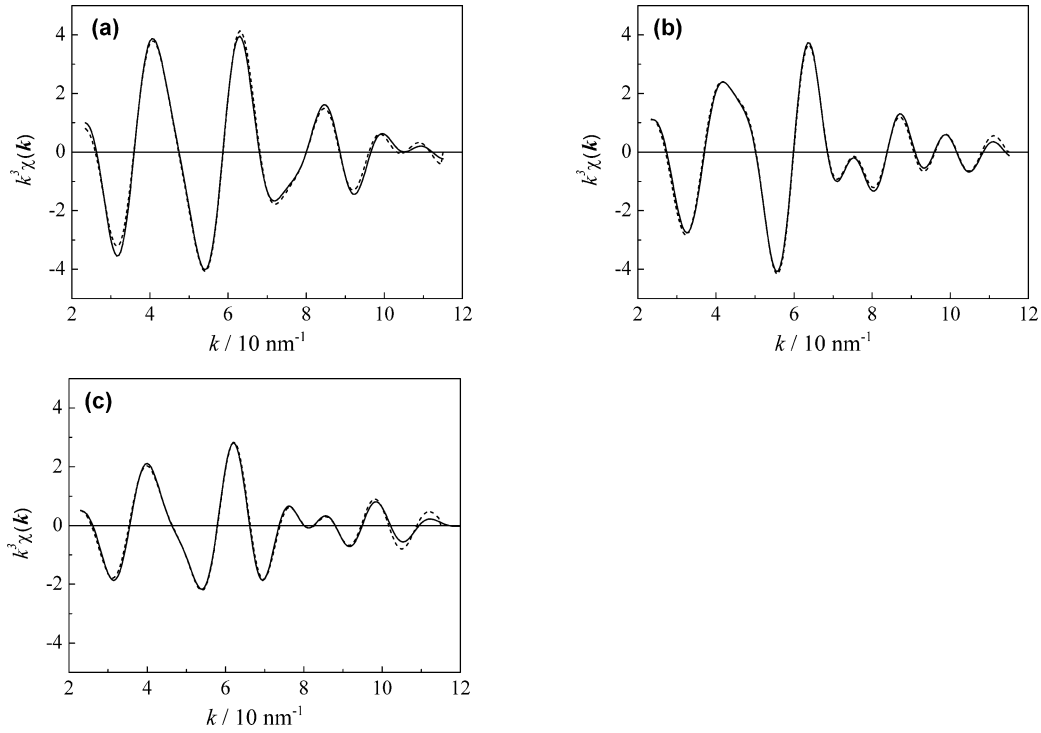

Fig. 13. Fourier filtered EXAFS data (solid line) and calculated data (dotted line) of Fe(0.40)-MFI after treatments with (a) O_2, (b) N_2O, and (c) H_2. Fitting results are listed in Table 3.

Table 3
Fe K-edge EXAFS fitting results for Fe(0.40)-MFI catalyst pretreated under different conditions

Shells	CN[a]	R[b] ($\times 10^{-1}$ nm)	σ[c] ($\times 10^{-1}$ nm)	ΔE_0[d] (eV)	R_f[e] (%)
Fe(0.40)-MFI after O_2 treatment[f]					
Fe–O_1	1.4 ± 0.1	1.90 ± 0.01	0.063 ± 0.013	-4.3 ± 1.1	0.54
Fe–O_2	2.5 ± 0.2	2.05 ± 0.01	0.078 ± 0.010	4.7 ± 0.8	
Fe–Si	1.5 ± 0.2	3.19 ± 0.01	0.060 ± 0.023	-5.3 ± 1.4	
Fe(0.40)-MFI after N_2O treatment[g]					
Fe–O_1	2.7 ± 0.1	1.89 ± 0.01	0.077 ± 0.007	5.5 ± 0.7	0.44
Fe–O_2	2.3 ± 0.1	2.05 ± 0.01	0.066 ± 0.010	0.6 ± 0.8	
Fe–Si	1.5 ± 0.2	3.19 ± 0.01	0.057 ± 0.022	-9.8 ± 1.3	
Fe–Fe	0.6 ± 0.1	2.95 ± 0.01	0.059 ± 0.021	3.0 ± 1.7	
Fe(0.40)-MFI after H_2 treatment[h]					
Fe–O_1	0.9 ± 0.1	1.89 ± 0.01	0.077 ± 0.023	4.6 ± 2.1	0.90
Fe–O_2	2.3 ± 0.2	2.06 ± 0.01	0.074 ± 0.010	0.6 ± 0.8	
Fe–Si	0.9 ± 0.2	3.22 ± 0.02	0.064 ± 0.039	-2.9 ± 2.3	
Fe–Fe	0.4 ± 0.1	2.91 ± 0.02	0.060 ± 0.031	-13.7 ± 2.6	

[a] Coordination number.
[b] Distance.
[c] Debye–Waller factor.
[d] Difference in the origin of photoelectron energy between the reference and the sample.
[e] Residual factor.
[f] Fourier filtering range: 0.077–0.298 nm.
[g] Fourier filtering range: 0.083–0.304 nm.
[h] Fourier filtering range: 0.080–0.304 nm.

more easily. In the case of Fe(0.40)-MFI, N_2O treatment can make the Fe structure change, and this is not the case with Fe(0.10)-MFI. The difference was clearly observed in the FT spectra. N_2O treatment decreased the peak intensity at 0.1–0.2 nm, and, in contrast, it increased the peak intensity at 0.2–0.3 nm. N_2O treatment increased the O_2 desorption amount from the TPD profiles; however, the peak intensity due to the Fe–O bond decreased. According to our curve-fitting analysis, the increase in the contribution of Fe–O_1 can explain this behavior. On the other hand, in the FT peak at the larger region, we added the Fe–Fe bond, because of the oscillation difference at the higher k region. Four-shell fitting

of Fe(0.40)-MFI after N_2O treatment requires 16 parameters, and this cannot be allowed on the basis of the limitation of the independent parameters (N_I) [44]. Here, N_I can be calculated to be 15.3 from $\Delta k = 91\ \mathrm{nm}^{-1}$, $\Delta R = 0.23$ nm. For the profile of Fe(0.40)-MFI after O_2 treatment, the best fitting result was obtained by a three-shell fitting. However, we could not obtain good fitting results for Fe(0.40)-MFI after N_2O treatment by the three-shell fitting. As a result, the curve fitting was carried out with two Fe–O, one Fe–Si, and one Fe–Fe shells. The results are listed in Table 3. Considering also other characterization results from H_2-TPR and O_2-TPD, it is strongly suggested that binuclear Fe species are formed on Fe(0.40)-MFI.

From the results of EXAFS studies, many research groups have reported various structures of Fe species prepared by different methods [24–33]. Sachtler et al. [30–32] reported that Fe/MFI prepared by a sublimation method has a molar ratio of Fe to Al-centered tetrahedral of 1:1 and that active species over MFI are oxygen-bridged binuclear iron species. Koningsberger et al. [24–26] determined the structure of the Fe binuclear complex with Fe–O–Fe bridges on Fe/ZSM-5 catalyst, which was prepared with $FeCl_3$ by EXAFS. Prins et al. [27,28] reported that the diiron structure resembles the core unit in methane monooxygenase (MMO). In addition, Panov et al. [29] indicated that α-oxygen can participate in the direct catalytic oxidation of benzene to phenol by N_2O over Fe-MFI, and the oxygen species are related to the presence of binuclear Fe complex. These reports suggest that the Fe species with the coordination of 0.25–0.30 nm are binuclear. On the other hand, Joyner et al. [33] reported the presence of very small iron–oxygen clusters of unusual structure such as Fe_4O_4, with a short iron–iron distance of ca. 0.25 nm. However, we could not observe the short Fe–Fe bond in EXAFS spectra. This can be interpreted that there are no iron-oxo nanoclusters such as Fe_4O_4 on our Fe-MFI catalysts, and this is also supported by H_2-TPR, in which no H_2 consumption due to Fe oxide was observed (see Fig. 8). In the previous H_2-TPR study, H_2 consumption with the peak at 850 K was observed on Fe_2O_3 [19]. Although the presence of oligonuclear Fe species is possible (binuclear, trinuclear, etc.), highly aggregated oligonuclear Fe species can be ruled out, because the Fe–Fe coordination number is determined to be 0.6 after N_2O treatment, which is clearly less than unity (Table 3). This also indicates that binuclear Fe species and isolated Fe ions are present. This interpretation is also supported by O_2-TPD and H_2-TPR: binuclear iron species are more reducible, and they give lower-temperature O_2 desorption. In addition, the coordination number of the Fe–O_1 shell was larger after N_2O treatment than that after O_2 treatment. This behavior can be explained by oxygen deposition on the Fe species by N_2O treatment (see Fig. 6).

The sum of Fe–O coordination is 5.0, which indicates Fe ion species are octahedrally coordinated with zeolite lattice oxygen, bridged oxygen, and OH ligands. In a previous report [25] it is shown that Fe binuclear species have an octahedral environment. These results also support that Fe binuclear species are present on our Fe(0.40)-MFI catalyst. However, we could not observe the Fe–Fe bond in Fe(0.40)-MFI after O_2 treatment. It seems that some of the bridged oxygen on binuclear Fe species is not present on Fe(0.40)-MFI after O_2 treatment. In contrast, an Fe–Fe bond is formed by N_2O treatment, and this is due to bridging of two Fe ions induced by deposited oxygen during the N_2O treatment. From the H_2-TPR profile, it is found that all of the iron species can be reduced from Fe^{3+} to Fe^{2+} with H_2 reduction at 773 K. After H_2 treatment (Fig. 13c), the coordination number of Fe–O_1 decreased because of oxygen removal during H_2 treatment (see Table 3). This behavior is observed more significantly in Fe–O_1. On the other hand, the coordination number of the Fe–O_2 shell, which can be assigned to the bond between Fe and lattice oxygen, was almost constant. This can be inferred from the presence of the oxygen species, which is hardly removed even after H_2 treatment.

3.4. Relation between catalyst structure and performance in N_2O reduction

From the results of EXAFS analysis combined with other characterization, it is found that Fe(0.40)-MFI contains binuclear and mononuclear Fe species, and Fe(0.10)-MFI contains only a mononuclear species. In the case of N_2O reduction with H_2, CO, and CH_4, TOF increased with increasing Fe loading, and this can be due to the formation of binuclear Fe species. From the comparison with H_2-TPR and O_2-TPD, more reducible Fe species are also assigned to binuclear Fe species.

The effect of reductants on N_2O reduction activity over Fe(0.40)-MFI is interesting in terms of the effectiveness of methane. Generally speaking, the reactivity of methane is very low compared with H_2 and CO. However, methane can play an important role for the reductant at almost the same temperature range as H_2 and CO. Pérez-Ramírez et al. [45] proposed that the $N_2O + CO$ reaction proceeds by a different mechanism on the different Fe ion species. Mononuclear Fe^{3+} species participated in this reaction via coordinated CO species on Fe^{3+} ions, and their oxidation state was not changed during the reaction. The reaction over oligonuclear Fe_xO_y clusters proceeds via a redox Fe^{3+}/Fe^{2+} process through the formation of O^- species as a reaction intermediate. Here, the Fe^{3+} in oligonuclear Fe_xO_y clusters can easily be reduced by CO. Therefore, they have concluded that active sites of $N_2O + CO$ reaction are oligonuclear Fe_xO_y clusters [45]. In our case, no formation of oligonuclear Fe_xO_y clusters was observed on the basis of H_2-TPR. The structure sensitivity of $N_2O + CO$ in our case can be explained by the reducibility of binuclear Fe species.

We can also conclude that the $N_2O + H_2$ reaction is also structure-sensitive and the behavior is similar to that of the $N_2O + CO$ reaction. In the case of the $N_2O + H_2$ reaction, the structure sensitivity can be related to the results

from H_2-TPR (Fig. 8), which indicate that the reducibility of Fe species increased with increasing Fe loading and the formation of Fe binuclear species. The structure sensitivity can also be inferred from the more reducible Fe binuclear species, which gives higher TOF.

In this work, we have shown that CH_4 is the most effective reductant in the presence and absence of excess oxygen. From the result of in situ FTIR study [20], we observed methoxy species formation during the $N_2O + CH_4$ reaction on a Fe-BEA catalyst. From the result of pulse reactions, we have proposed that formation of methoxy species promotes the reduction of Fe ion species on the active sites, which are suggested to be binuclear Fe species [19]. In addition, higher TOF was observed in the $N_2O + CH_4$ reaction (Fig. 9d) over Fe-MFI with higher Fe loading. These results indicate that the structure sensitivity of the $N_2O + CH_4$ reaction can be related to the formation of methoxy species from methane activated with oxygen supplied by N_2O dissociation over binuclear Fe species [19].

4. Conclusions

1. In the selective catalytic reduction (SCR) of N_2O with hydrocarbons in the presence of excess O_2, CH_4 and C_2H_6 were not activated by O_2 but by N_2O, although C_3H_6 could react with oxygen. The order of N_2O contribution in the SCR under excess oxygen is $CH_4 > C_2H_6 > C_3H_6$. This means that CH_4 is a more efficient reductant for the SCR of N_2O.
2. The TOFs of N_2O reduction by H_2, CO, and CH_4 and N_2O decomposition in the absence of oxygen increased with increasing molar ratio of Fe/Al, when Fe/Al is above 0.15, whereas TOFs were lower and constant in the range of $Fe/Al \leqslant 0.10$.
3. From H_2-TPR, more reducible Fe species were formed over Fe-MFI with higher Fe loading. In O_2-TPD, Fe(0.40)-MFI had oxygen species that could be desorbed at lower temperatures than Fe(0.10)-MFI.
4. From the result of EXAFS analysis, only mononuclear Fe species were observed over Fe(0.10)-MFI after treatment with O_2 or N_2O. On the other hand, binuclear Fe species and mononuclear Fe species were observed over Fe(0.40)-MFI after treatment with N_2O or H_2. More reducible Fe species, which gave lower-temperature O_2 desorption, can be due to Fe binuclear species over Fe(0.40)-MFI.
5. Although the reactivity of methane is usually very low, CH_4 can be oxidized by N_2O more easily than by H_2 and CO. Formation of methoxy species on the Fe ion species promotes the reduction of Fe ion sites even in excess oxygen, and this can promote the redox cycle of binuclear Fe species.

Acknowledgments

A part of this research was supported by the Research Institute of Innovative Technology for the Earth (RITE) and a Center of Excellence Grant-in-aid for the 21st Century COE Program for Frontiers from the Ministry of Education, Culture, Sports, Science and Technology. This work was performed under the approval of the Photon Factory Advisory Committee (Proposal No. 2003G255). The authors are grateful to the Chemical Analysis Center, University of Tsukuba, for ICP analysis of Fe-MFI catalysts.

References

[1] F. Kapteijn, J. Rodrigues-Mirasol, J.A. Moulijn, Appl. Catal. B 9 (1996) 25.
[2] M. Nakamura, H. Mitsuhashi, N. Takezawa, J. Catal. 138 (1992) 686.
[3] S. Tanaka, K. Yuzaki, S. Ito, S. Kameoka, K. Kunimori, J. Catal. 200 (2001) 203.
[4] X.F. Wang, H.C. Zeng, Appl. Catal. B 17 (1998) 89.
[5] G. Centi, L. Dall'Olio, S. Perathoner, J. Catal. 192 (2000) 224.
[6] Y. Li, J.N. Armor, Appl. Catal. B 1 (1992) L21.
[7] T. Turek, Appl. Catal. B 9 (1996) 201.
[8] J. Leglise, J.O. Petunchi, W.K. Hall, J. Catal. 86 (1984) 392.
[9] T. Nobukawa, S. Tanaka, S. Ito, K. Tomishige, S. Kameoka, K. Kunimori, Catal. Lett. 83 (2002) 5.
[10] J. Pérez-Ramírez, F. Kapteijn, G. Mul, J.A. Moulijn, J. Catal. 208 (2002) 211.
[11] G. Centi, F. Vazzana, Catal. Today 53 (1999) 683.
[12] R.W. van den Brink, S. Booneveld, J.R. Pels, D.F. Bakker, M.J.F.M. Verhaak, Appl. Catal. B 32 (2001) 73.
[13] K. Yamada, S. Kondo, K. Segawa, Mocropor. Mesopor. Mater. 35–36 (2000) 227.
[14] A. Satsuma, H. Maeshima, K. Watanabe, K. Suzuki, T. Hattori, Catal. Today 63 (2000) 347.
[15] S. Kameoka, T. Suzuki, K. Yuzaki, T. Takeda, S. Tanaka, S. Ito, T. Miyadera, K. Kunimori, Chem. Commun. (2000) 745.
[16] S. Kameoka, K. Yuzaki, T. Takeda, S. Tanaka, S. Ito, T. Miyadera, K. Kunimori, Phys. Chem. Chem. Phys. 3 (2001) 256.
[17] S. Kameoka, K. Kita, S. Tanaka, T. Nobukawa, S. Ito, K. Tomishige, T. Miyadera, K. Kunimori, Catal. Lett. 79 (2002) 63.
[18] S. Kameoka, T. Nobukawa, S. Tanaka, S. Ito, K. Tomishige, K. Kunimori, Phys. Chem. Chem. Phys. 5 (2003) 3328.
[19] M. Yoshida, T. Nobukawa, S. Ito, K. Tomishige, K. Kunimori, J. Catal. 223 (2004) 454.
[20] T. Nobukawa, M. Yoshida, S. Kameoka, S. Ito, K. Tomishige, K. Kunimori, J. Phys. Chem. B 108 (2004) 4071.
[21] B. Coq, M. Mauvezin, G. Delahay, S. Kieger, J. Catal. 195 (2000) 298.
[22] G. Delahay, M. Mauvezin, B. Coq, S. Kieger, J. Catal. 202 (2001) 156.
[23] G. Delahay, M. Mauvezin, A. Guzmán-Vargas, B. Coq, Catal. Commun. 3 (2002) 385.
[24] A.A. Battiston, J.H. Bitter, F.M.F. de Groot, A.R. Overweg, O. Stephan, J.A. van Bokhoven, P.J. Kooyan, C. van der Spek, G. Vankó, D.C. Koningsberger, J. Catal. 213 (2003) 251.
[25] A.A. Battiston, J.H. Bitter, W.M. Heijboer, F.M.F. de Groot, D.C. Koningsberger, J. Catal. 215 (2003) 279.
[26] A.A. Battiston, J.H. Bitter, D.C. Koningsberger, J. Catal. 218 (2003) 163.
[27] P. Marturano, L. Drozdová, A. Kogelbauer, R. Prins, J. Catal. 192 (2000) 236.
[28] P. Marturano, L. Drozdová, G.D. Pirngruber, A. Kogelbauer, R. Prins, Phys. Chem. Chem. Phys. 3 (2001) 5585.
[29] K.A. Dubkov, N.S. Ovanesyan, A.A. Shteinman, E.V. Starokon, G.I. Panov, J. Catal. 207 (2002) 341.

[30] H.-Y. Chen, W.M.H. Sachtler, Catal. Today 42 (1998) 73.
[31] H.-Y. Chen, El-M. El-Malki, X. Wang, R.A. van Santen, W.M.H. Sachtler, J. Mol. Catal. A 162 (2000) 159.
[32] El-M. El-Malki, R.A. van Santen, W.M.H. Sachtler, J. Catal. 196 (2000) 212.
[33] R. Joyner, M. Stockenhuber, J. Phys. Chem. B 103 (1999) 5963.
[34] W.N. Delgass, R.L. Garten, M. Boudart, J. Chem. Phys. 50 (1969) 4603.
[35] J.W. Cook, D.E. Sayers, J. Appl. Phys. 52 (1981) 5024.
[36] K. Okumura, J. Amano, N. Yasunobu, M. Niwa, J. Phys. Chem. B 104 (2000) 1050.
[37] K. Okumura, S. Matsumoto, N. Nishiaki, M. Niwa, Appl. Catal. B 40 (2003) 151.
[38] L. Ankudinov, B. Ravel, J.J. Rehr, S.D. Conradson, Phys. Rev. B (1998) 7565.
[39] B. Ravel, version 3.0beta8 4 March, The university of Washington, 2003.
[40] S. Kameoka, K. Yuzaki, T. Takeda, S. Tanaka, S. Ito, T. Miyadera, K. Kunimori, Phys. Chem. Chem. Phys. 3 (2001) 256.
[41] D.A. Bulushev, L. Kiwi-Minsker, A. Renken, J. Catal. 222 (2004) 389.
[42] G.D. Pirngruber, J. Catal. 219 (2003) 456.
[43] S.H. Choi, B.R. Wood, J.A. Ryder, A.T. Bell, J. Phys. Chem. B 107 (2003) 11843.
[44] E.A. Stern, Phys. Rev. B 48 (1993) 9825.
[45] J. Pérez-Ramírez, M.S. Kumar, A. Brückner, J. Catal. 223 (2004) 13.